



Oxygen vacancy enhanced catalytic activity of reduced Co_3O_4 towards *p*-nitrophenol reduction

Huihui Chen ^{a,b}, Mei Yang ^{a,*}, Sha Tao ^{a,b}, Guangwen Chen ^{a,*}

^a Dalian National Laboratory for Clean Energy, Dalian Institute of Chemical Physics, Chinese Academy of Sciences, Dalian 116023, China

^b University of Chinese Academy of Sciences, Beijing 100049, China

ARTICLE INFO

Article history:

Received 6 December 2016

Received in revised form 21 February 2017

Accepted 13 March 2017

Available online 20 March 2017

Keywords:

Co_3O_4
Reduced
Oxygen vacancy
p-Nitrophenol
 NaBH_4

ABSTRACT

With the aim of replacing noble metal-based catalysts, many efforts have been devoted to the development of highly active non-noble metal-based catalysts for the reduction of *p*-nitrophenol (*p*-NP) to *p*-aminophenol (*p*-AP) by NaBH_4 . As a typical transition metal oxide, pristine Co_3O_4 is normally considered to be poorly active towards the reduction of *p*-NP to *p*-AP. In this work, the catalytic activity of pristine Co_3O_4 was remarkably enhanced by a facile surface reduction with aqueous NaBH_4 . With the characterization results of various techniques such as XRD, TEM, H_2 -TPR and XPS, the enhancement in the catalytic activity was attributed to the oxygen vacancies generated during the surface reduction process. The catalytic activity of reduced Co_3O_4 was found to be strongly dependent on the reduction time and NaBH_4 concentration used for catalyst preparation. Through the surface reduction with 0.05 mol/L aqueous NaBH_4 for 40 min, the as-prepared reduced Co_3O_4 showed the best catalytic activity in term of the shortest induction time (<0.75 min) and highest mass-normalized rate constant ($20.86 \text{ min}^{-1} \text{ g}^{-1} \text{ L}$). Furthermore, the as-prepared reduced Co_3O_4 displayed no obvious deactivation during the five successive cycles.

© 2017 Elsevier B.V. All rights reserved.

1. Introduction

Nitroaromatic chemicals are one of the most common organic pollutants in industrial wastewater which are toxic, mutagenic and biorefractory. Taking *p*-nitrophenol (*p*-NP) as an example, the maximum contaminant level in natural water is 10 ng/L according to the guideline of United States Environmental Protection Agency due to its eye and skin irritation, kidney and liver injury, and methemoglobin formation, etc [1,2]. Therefore, tremendous efforts have been made to eliminate *p*-NP via low-cost, high-efficiency and environmental benign methods. One of the most feasible and versatile methods is the catalytic reduction of *p*-NP to *p*-aminophenol (*p*-AP) by NaBH_4 [3–8]. This reduction process is usually carried out at room temperature and the maximum contaminant level of *p*-AP in natural water is much larger than that of *p*-NP. More importantly, *p*-AP is an important intermediate material for the production of dyes, pharmaceuticals, agrochemicals, photographic developers and chelating agents, etc. In addition to the application in industrial wastewater treatment, the catalytic reduction of *p*-NP to *p*-AP with NaBH_4 has also been widely used as a model reaction to eval-

uate the catalytic performances of nanoparticles (NPs), particularly noble metal NPs.

Up to now, various kinds of noble metal NPs such as Au, Ag, Pd and Pt have been successfully synthesized and exhibited excellent activities in the catalytic reduction of *p*-NP to *p*-AP by NaBH_4 [9–14]. Experimentally, the catalytic performances of noble metal NPs are significantly affected by the size, shape and composition, etc. For example, Zhang et al. found that the catalytic activity decreased with the increasing thickness of two-dimensional Au nanosheets with a polygon morphology [15]. Min et al. reported that monodisperse Ag nanocages with specific interiors outperformed Ag NPs with the diameter of ca. 5 nm [16]. Unfortunately, despite noble metal NPs are highly active for the catalytic reduction of *p*-NP to *p*-AP by NaBH_4 , they are prone to aggregate during the reaction because of their high surface energy and Van der Waals forces. The irreversible aggregation of noble metal NPs inevitably leads to a decrease in the catalytic activity. Generally, three strategies have been adopted to overcome this drawback. In the first strategy, noble metal NPs are deposited on the supports to obtain high dispersion and good stability. Diversified supports such as Fe_3O_4 , SiO_2 , $\gamma\text{-Al}_2\text{O}_3$ and graphene have been used [17–21]. The second strategy is to stabilize noble metal NPs with surface bound ligands [22]. For example, Dai et al. employed amphiphilic hyperbranched polymers to stabilize Au NPs and the corresponding

* Corresponding authors.

E-mail addresses: yangmei@dicp.ac.cn (M. Yang), gwchen@dicp.ac.cn (G. Chen).

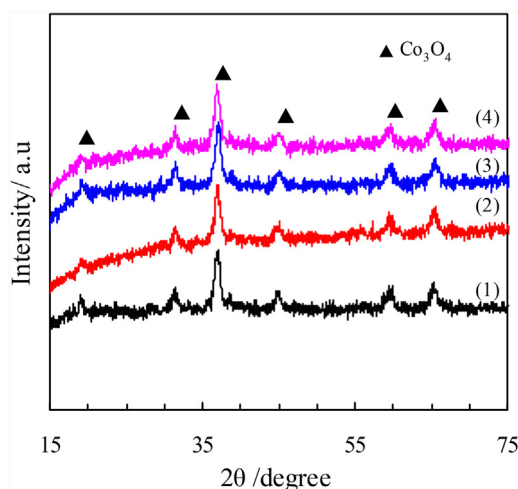


Fig. 1. The XRD patterns of (1) pristine Co_3O_4 (2) Co_3O_4 -0.05-10 (3) Co_3O_4 -0.05-20 (4) Co_3O_4 -0.05-40.

catalysts showed high catalytic activity for the reduction of p-NP to p-AP [23]. Nevertheless, it cannot be neglected that the surface bound ligands may block the active surface sites and eliminate catalytic activity. Ansar and Kitchens showed that high surface coverage of low molecular weight thiolated polyethylene glycol (1 kDa) totally inhibited the catalytic activity of Au NPs [24]. In the third one, noble metal NPs are preserved by core-shell or alloy nanostructures such as $\text{Au-CeO}_2@ \text{ZrO}_2$, $\text{Au@mesoporous SnO}_2$, AuPt and AuPd bimetallic NPs, etc [25–30].

Besides noble metal NPs-based catalysts, metallic Co-based catalysts have received increasing attention owing to their low costs [31]. As an example, Ma et al. demonstrated the Co NPs supported on two-dimensional MgAl layered double oxide nanodisks were highly active with the mass-normalized rate constant of

$83 \text{ min}^{-1} \text{ g}^{-1} \text{ L}$ [32]. Yan et al. reported that Co@SiO_2 nanorattles exhibited both good catalytic activity and stability [33]. Wu et al. found that $\text{Ni}_{33.8}\text{Co}_{66.2}$ dendrites were more active than the flowerlike $\text{Ni}_{33.4}\text{Co}_{66.6}$ due to the larger surface-to-volume ratio and surface area [34]. Notably, Co_3O_4 was also found to be active for the catalytic reduction of p-NP to p-AP by NaBH_4 [35,36]. However, the catalytic activities of Co_3O_4 reported in the literature studies were always much lower than those of noble metal NPs-based and metallic Co-based catalysts.

It has been found that the physicochemical properties of metal oxides were affected dramatically by the oxygen vacancies [37]. Through precise and controlled introduction of oxygen vacancies, the catalytic performances of metal oxides can be enhanced to a large extent [38–41]. Motivated by the enhancement effect, we aimed to improve the catalytic activity of pristine Co_3O_4 by introducing a moderate amount of oxygen vacancies in this paper. The oxygen vacancies were introduced by annealing pristine Co_3O_4 in aqueous NaBH_4 (surface reduction). This method has been widely employed to create oxygen vacancies on the surfaces of metal oxides [42,43]. As expected, the catalytic activity of pristine Co_3O_4 was remarkably improved. The improved catalytic activity was evidenced to be closely related with the oxygen vacancies created during the surface reduction process. Co_3O_4 reduced in 0.05 mol/L aqueous NaBH_4 for 40 min possessed the largest amount of oxygen vacancies and thus best catalytic performance.

2. Experimental section

2.1. Materials

Cobalt chloride ($\text{CoCl}_2 \cdot 2\text{H}_2\text{O}$), sodium hydroxide (NaOH), sodium borohydride (NaBH_4) and *p*-nitrophenol ($\text{C}_6\text{H}_5\text{NO}_3$) were purchased with analytical grade. All chemicals were used as received without further treatment. Deionized water was used in all experiments.

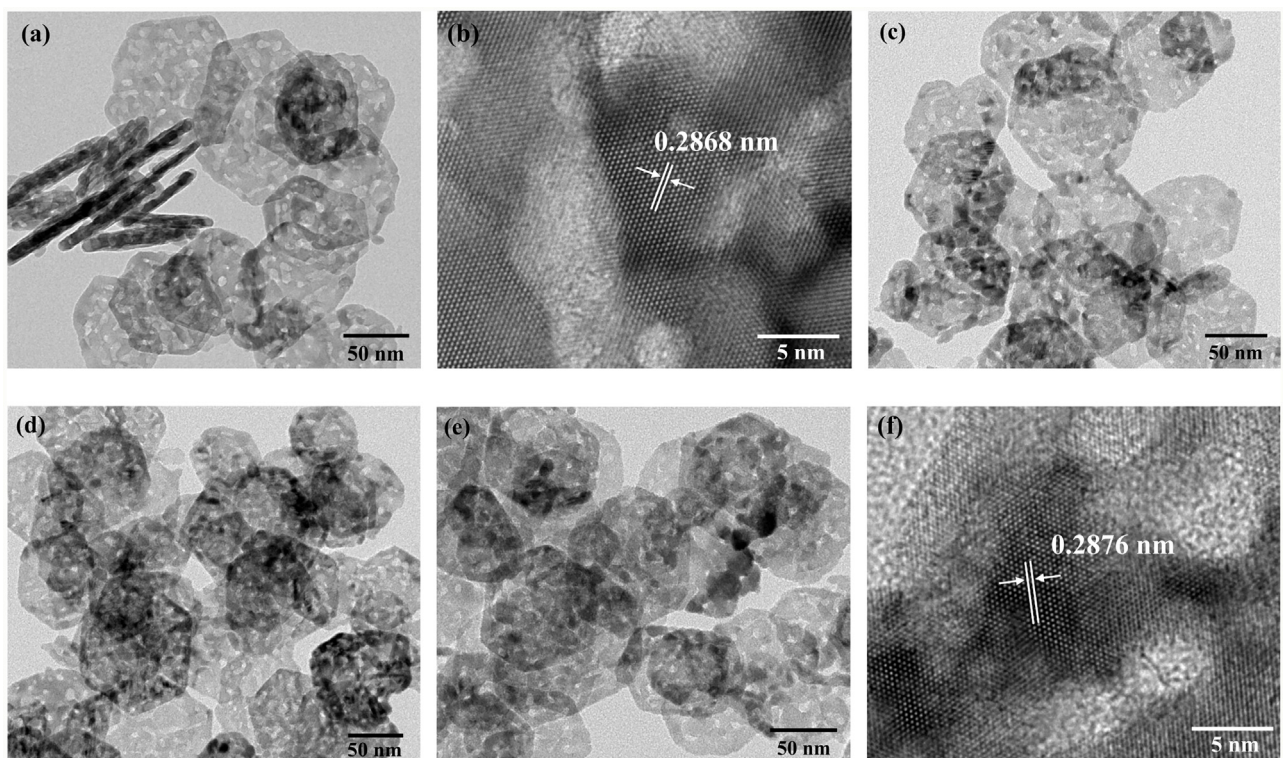


Fig. 2. The TEM images of (a, b) pristine Co_3O_4 (c) Co_3O_4 -0.05-10 (d) Co_3O_4 -0.05-20 (e, f) Co_3O_4 -0.05-40.

2.2. The preparation of pristine and reduced Co_3O_4

In a typical experiment, $\text{CoCl}_2 \cdot 2\text{H}_2\text{O}$ (5 mmol) and NaOH (50 mmol) were dissolved into 50 mL deionized water, respectively. The precipitation process was carried out by dropwise addition of CoCl_2 and NaOH aqueous solutions into a stirred three-necked flask containing 50 mL deionized water at 50 °C under N_2 atmosphere. A pink suspension was obtained and kept at 50 °C for 1 h. Subsequently, N_2 flow was stopped. After being cooled to room temperature, the pink precipitate was centrifuged, washed several times with deionized water and dried at 100 °C overnight. The as-prepared pink precipitate was calcined at 300 °C for 2 h in air to obtain pristine Co_3O_4 .

The reduced Co_3O_4 was prepared by soaking pristine Co_3O_4 powder in aqueous NaBH_4 at 30 °C. After a certain time, the powder was centrifuged, washed several times with deionized water and used for the catalytic reduction of p-NP to p-AP directly. The as-prepared reduced Co_3O_4 was denoted as $\text{Co}_3\text{O}_4\text{-X-Y}$, where X and Y represented the concentration of aqueous NaBH_4 used for catalyst preparation (mol/L) and reducing time (min), respectively.

2.3. Catalyst characterization

The powder X-ray diffraction (XRD) patterns of the as-prepared samples were recorded by a PANalytical X'pert-Pro powder X-ray diffractometer, using Cu Ka monochromatized radiation ($\lambda = 0.1541 \text{ nm}$) at a scanning rate of 5°/min.

The specific surface areas and pore properties of the as-prepared samples were measured on a Quadasorb SI instrument using nitrogen adsorption isotherms at 77 K (the cross section of the nitrogen molecule was taken to 0.162 nm²).

The morphologies of the as-prepared samples were observed by transmission electron microscopy (TEM, JEOL JEM-2100) with the accelerating voltage of 120 kV and scanning electron microscopy (SEM, JEOL JSM-7800F) with the accelerating voltage of 3 kV.

Temperature programmed reduction ($\text{H}_2\text{-TPR}$) was performed on a Micromeritics AutoChem 2920 apparatus. 100 mg of pristine Co_3O_4 was placed into a quartz U tube, and then heated at 300 °C for 2 h in Ar. Subsequently, the temperature was lowered to 50 °C and Ar was replaced by $\text{H}_2\text{/Ar}$. Then, the temperature was programmed to increase from 50 to 700 °C with the heating rate of 10 °C/min.

X-ray photoelectron spectroscopy (XPS) analysis was performed on an ESCALAB 250Xi system, using Al Ka radiation as the X-ray source, which was used to analyze elemental composition and chemical state of the as-prepared samples.

2.4. Catalytic reduction of p-NP to p-AP by NaBH_4

The catalytic reduction of p-NP to p-AP by NaBH_4 was carried out at room temperature (23 °C) in a standard quartz cell with a volume of 3.5 mL. Firstly, 2.0 mL p-NP aqueous solution (0.175 mmol/L) was mixed with 0.7 mL fresh NaBH_4 solution (0.01–0.05 mol/L) in the quartz cell. Then, 0.1 mL suspension containing the as-prepared catalyst (2 g/L) was injected to the mixture quickly to start the reduction. The reduction process was monitored by an in-situ UV-vis spectrophotometer (METASH UV8000) over a scanning range of 200–550 nm. The catalytic activity was measured by the extinction of the absorption peak of p-NP at 400 nm as a function of reaction time. The reusability of as-prepared catalyst was investigated by five successive cycles of the catalytic reduction of p-NP to p-AP by NaBH_4 .

Table 1

The BET surface areas and pore volumes of pristine and reduced Co_3O_4 .

Sample	BET surface area (m ² /g)	Pore volume (cc/g)
Pristine Co_3O_4	106	0.27
$\text{Co}_3\text{O}_4\text{-0.05-10}$	86	0.30
$\text{Co}_3\text{O}_4\text{-0.05-20}$	94	0.24
$\text{Co}_3\text{O}_4\text{-0.05-40}$	95	0.21

3. Results and discussion

3.1. Catalyst characterization

3.1.1. XRD

Fig. 1 shows the XRD patterns of pristine Co_3O_4 and Co_3O_4 reduced for different times. The diffraction peaks at 19.155°, 31.355°, 36.993°, 44.934°, 59.542° and 65.332° in the XRD pattern of pristine Co_3O_4 can be assigned to the (1 1 1), (2 2 0), (3 1 1), (4 0 0), (4 2 2) and (4 4 0) facets of cubic Co_3O_4 , respectively (JCPDS No. 43-1003). For $\text{Co}_3\text{O}_4\text{-0.05-Y}$ (Y = 10, 20 and 40 min), only the characteristic diffraction peaks of cubic Co_3O_4 are found, indicating that the crystal structure of pristine Co_3O_4 is well preserved during the surface reduction process. No diffraction peaks belonging to CoO (JCPDS No. 42-1300) or metallic Co (JCPDS No. 15-0806) are found. This indicates that no CoO or metallic Co are formed, or their contents are below the detection limitation of XRD. To further identify the chemical state of Co element, XPS analysis was carried out and the results will be discussed in the following section. According to Scherrer's equation, the crystalline size of cubic Co_3O_4 is 11.9 nm for pristine Co_3O_4 , while that is 14.3 nm in the case of $\text{Co}_3\text{O}_4\text{-0.05-Y}$ (Y = 10, 20 and 40 min). This implies that the crystalline size of cubic Co_3O_4 increases during the surface reduction process but is independent of the reduction time.

3.1.2. N_2 physisorption

The specific surface areas of pristine and reduced Co_3O_4 based on BET method are summarized in Table 1. Pristine Co_3O_4 possesses the largest specific surface area of 106 m²/g among all the samples. Reducing pristine Co_3O_4 with aqueous NaBH_4 results in a decrease in the specific surface area. The pore volumes of pristine and reduced Co_3O_4 are very similar, ranging from 0.21 to 0.30 cc/g. The N_2 adsorption-desorption isotherm curves and BJH adsorption pore size distributions of pristine and reduced Co_3O_4 are shown in Fig. S1. Pristine and reduced Co_3O_4 all exhibit a Type IV adsorption isotherm with an H_1 hysteresis loop, indicating the disordered mesoporous nature. The pore size distributions derived from adsorption branch of pristine and reduced Co_3O_4 show a broad distribution from 3.5 nm to 65 nm, which can be attributed to the intra-aggregated pore within the agglomerated particles.

3.1.3. TEM and SEM

TEM and SEM were performed to visually observe the morphology of the as-prepared samples. Figs. 2 and 3 depict the TEM and SEM images of pristine Co_3O_4 and Co_3O_4 reduced for different times. As shown in Figs. 2 a and 3 a, pristine Co_3O_4 is mainly composed of well-defined hexagonal nanoplates with an average edge length of ~100 nm and thickness of ~20 nm. It is evident that there are many pores with the diameter ranging from 5 to 10 nm on the nanoplates, which are formed due to the dehydration of $\beta\text{-Co(OH)}_2$ to Co_3O_4 . Fig. 2b shows the HRTEM image of pristine Co_3O_4 . As shown in Fig. 2b, the lattice fringes with an interplanar spacing of 0.29 nm can be attributed to the (2 2 0) facets of cubic Co_3O_4 , in good accordance with the XRD result. When pristine Co_3O_4 is reduced by aqueous NaBH_4 , the morphology of pristine Co_3O_4 is well maintained (Figs. 2 c–e and 3 b–d). $\text{Co}_3\text{O}_4\text{-0.05-Y}$ (Y = 10, 20 and 40 min) all consist of hexagonal nanoplates. No cracking of

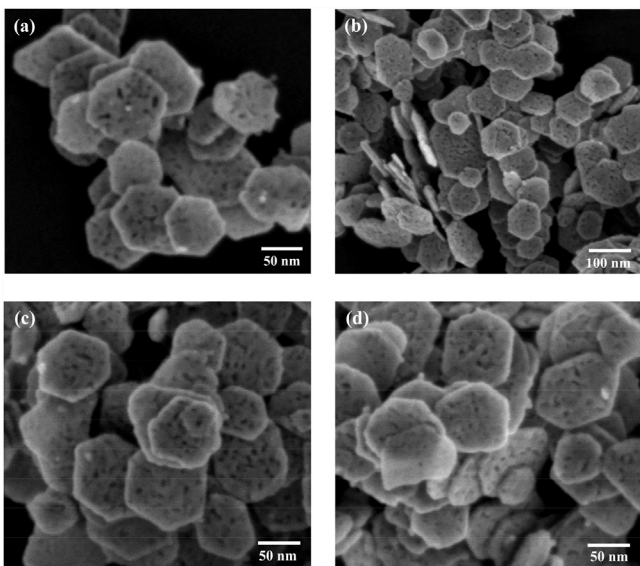


Fig. 3. The SEM images of (a) pristine Co_3O_4 (b) Co_3O_4 -0.05-10 (c) Co_3O_4 -0.05-20 (d) Co_3O_4 -0.05-40.

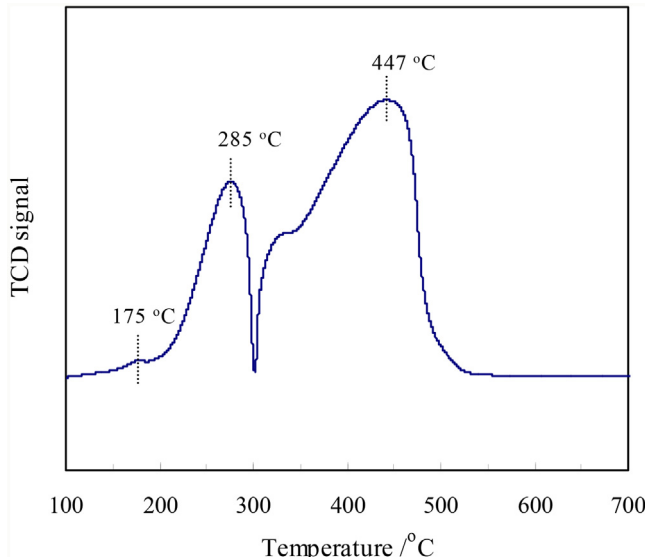


Fig. 4. H_2 -TPR profile of pristine Co_3O_4 .

hexagonal nanoplates occurs during the surface reduction process. As shown in Fig. 2f, the lattice fringes with an interplanar spacing of 0.29 nm is obtained for Co_3O_4 -0.05-40, indicating the preservation of cubic Co_3O_4 crystal structure during the surface reduction process.

3.1.4. H_2 -TPR

H_2 -TPR was conducted to study the redox property of pristine Co_3O_4 . In previous studies, it was found that the reduction behavior of Co_3O_4 strongly depended on the preparation method, catalyst composition and dispersion [44,45]. The reduction behavior of Co_3O_4 was widely accepted as a stepwise process including the reduction of Co^{3+} to Co^{2+} and Co^{2+} to Co [46]. Fig. 4 shows the H_2 -TPR profile of pristine Co_3O_4 . Evidently, the reduction behavior of pristine Co_3O_4 is similar with those reported in previous studies. As shown in Fig. 4, the H_2 -TPR profile of pristine Co_3O_4 has two distinct peaks. The peak centered at 285 °C can be attributed to the transformation of Co^{3+} to Co^{2+} , while the other peak centered at 447 °C is caused by the reduction of Co^{2+} to Co. The area ratio of

Table 2
The molar percentages of Co^{2+} and Co^{3+} in pristine and reduced Co_3O_4 .

Sample	Co^{2+} (mol%)	Co^{3+} (mol%)
pristine Co_3O_4	32.5	67.5
Co_3O_4 -0.05-10	32.8	67.2
Co_3O_4 -0.05-20	33.5	66.5
Co_3O_4 -0.05-40	34.3	65.7

the two peaks is calculated to be 1:3.2, which is close to the stoichiometric ratio of Co^{3+} to Co^{2+} in Co_3O_4 . This further proves the stepwise reduction of pristine Co_3O_4 . In addition, the small peak at 175 °C can be ascribed to the reduction of the surface adsorbed oxygen species [47].

3.1.5. XPS

The aforementioned characterization techniques including XRD, N_2 physisorption, TEM, SEM and H_2 -TPR mainly reflected the physicochemical properties of bulk phase. Apparently, no obvious changes occurred for the bulk phase of pristine Co_3O_4 during the surface reduction process. We can predict that reducing pristine Co_3O_4 with aqueous NaBH_4 might result in a surface change. In fact, a surface change in term of the formation of oxygen vacancies has been extensively found after treating metal oxides with aqueous NaBH_4 . For example, Kang et al. reported that NaBH_4 treatment introduced oxygen vacancies on the surface and interior of TiO_2 nanotube arrays [42]. Wang et al. observed that treating Co_3O_4 nanowires with aqueous NaBH_4 resulted in an increasing amount of oxygen vacancies on the surface [48]. It is widely accepted that the oxygen vacancies are formed due to the reduction of higher valent metal ions (Ti^{4+} , W^{6+} , Co^{3+}) to lower valent metal ions (Ti^{3+} , W^{5+} , Co^{2+}). Therefore, the relative content of lower valent metal ions is an important indicator for the amount of oxygen vacancies. In this section, XPS analysis was carried out to investigate the chemical state of Co element to deduce whether the same change occurred on the surface of pristine Co_3O_4 . Fig. 5a shows the scan survey spectra of pristine Co_3O_4 and Co_3O_4 reduced for different times. It is apparent that every peak on the spectra can be ascribed to Co, O or C elements without any impurities. Generally, the presence of C element can be attributed to the hydrocarbon contaminants inherently existing in the XPS analysis. Therefore, the XPS spectra suggest that pristine and reduced Co_3O_4 are merely constituted of Co and O elements. No characteristic peaks assigned to B element are observed, indicating the absence of Co_xB . Co_xB has been identified as the active species and was in-situ formed in the hydrolysis of NaBH_4 with Co_3O_4 as the catalyst [49,50]. The absence of Co_xB can be ascribed to the low NaBH_4 concentration used for catalyst preparation. The high-resolution XPS spectra of Co element is displayed in Fig. 5b. For pristine Co_3O_4 , the peaks located at 781.7 and 796.8 eV are ascribed to Co^{2+} , while the other two peaks located at 780.0 and 795.1 eV correspond to Co^{3+} . Obviously, Co element exists in the chemical state of Co^{2+} and Co^{3+} . No characteristic peaks corresponding to metallic Co are detected, indicating that aqueous NaBH_4 is unable to reduce Co^{2+} to metallic Co under the present condition. In the case of Co_3O_4 -0.05-Y (Y = 10, 20 and 40 min), the high-resolution XPS spectra of Co element can be also deconvoluted into the characteristic peaks of Co^{2+} and Co^{3+} . The molar percentages of Co^{2+} and Co^{3+} are summarized in Table 2. As shown in Table 2, the molar percentage of Co^{2+} increases with the increasing reduction time, implying a portion of Co^{3+} is reduced to Co^{2+} by aqueous NaBH_4 . This is consistent with the H_2 -TPR profile of pristine Co_3O_4 , in which the reduction of Co^{3+} to Co^{2+} is much easier than that of Co^{2+} to Co. According to the study of Wang et al., the reduction of Co^{3+} to Co^{2+} could result in the formation of oxygen vacancies [48]. Consequently, it can be predicted that oxygen vacancies are created by treating pristine Co_3O_4 with aqueous NaBH_4 . Furthermore, the amount of oxygen vacan-

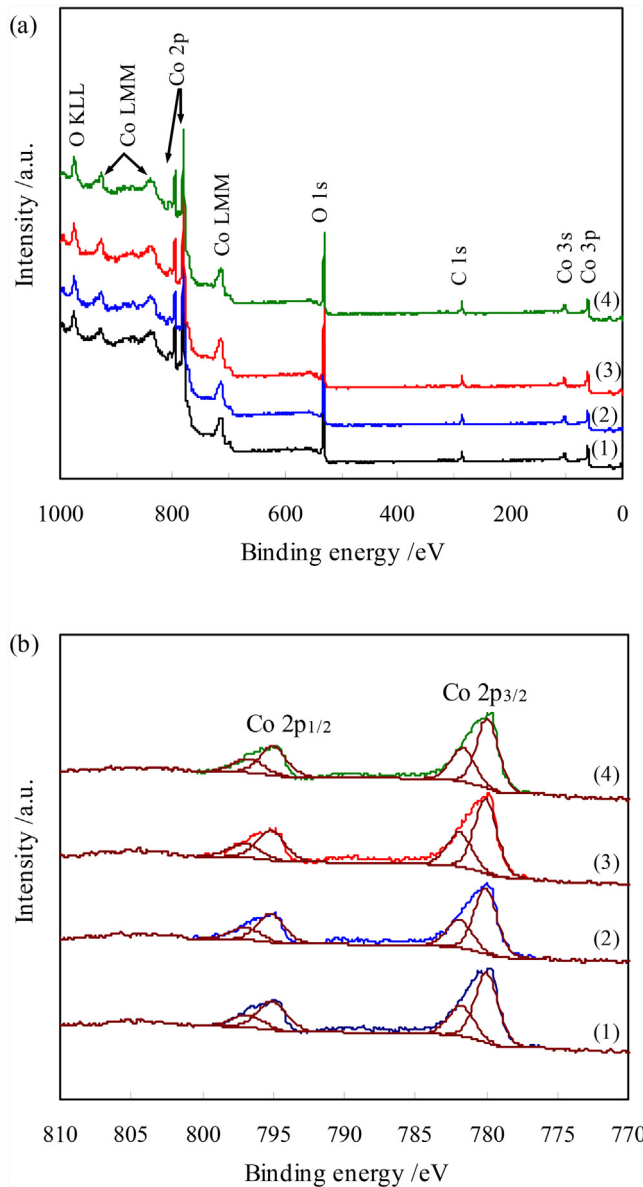


Fig. 5. (a) XPS survey spectra (b) Co 2p spectra of (1) pristine Co_3O_4 (2) Co_3O_4 -0.05-10 (3) Co_3O_4 -0.05-20 (4) Co_3O_4 -0.05-40.

cies on the surface of reduced Co_3O_4 increases with the increase in reduction time.

3.2. Catalytic reduction of p-NP to p-AP by NaBH_4

The catalytic reduction of p-NP to p-AP by NaBH_4 was carried out in a standard quartz cell and monitored by an in situ UV-vis spectrophotometer. As shown in Fig. S2, p-NP exhibits a strong absorption peak centered at 317 nm. After the addition of NaBH_4 , the absorption peak shifts to 400 nm due to the formation of p-NP anions, accompanied with the solution color changing from light yellow to green yellow. The reduction of p-NP to p-AP by NaBH_4 does not occur in the absence of catalyst due to the large difference in the redox potential of the donor and acceptor couple. After the addition of reduced Co_3O_4 , the absorption peak of p-NP anions at 400 nm gradually decreases, and correspondingly a new absorption peak appears at 300 nm, which can be attributed to the formation of p-AP. In this section, the effects of reduction time, NaBH_4 concentration used for catalyst preparation, molar ratio of NaBH_4 to p-NP

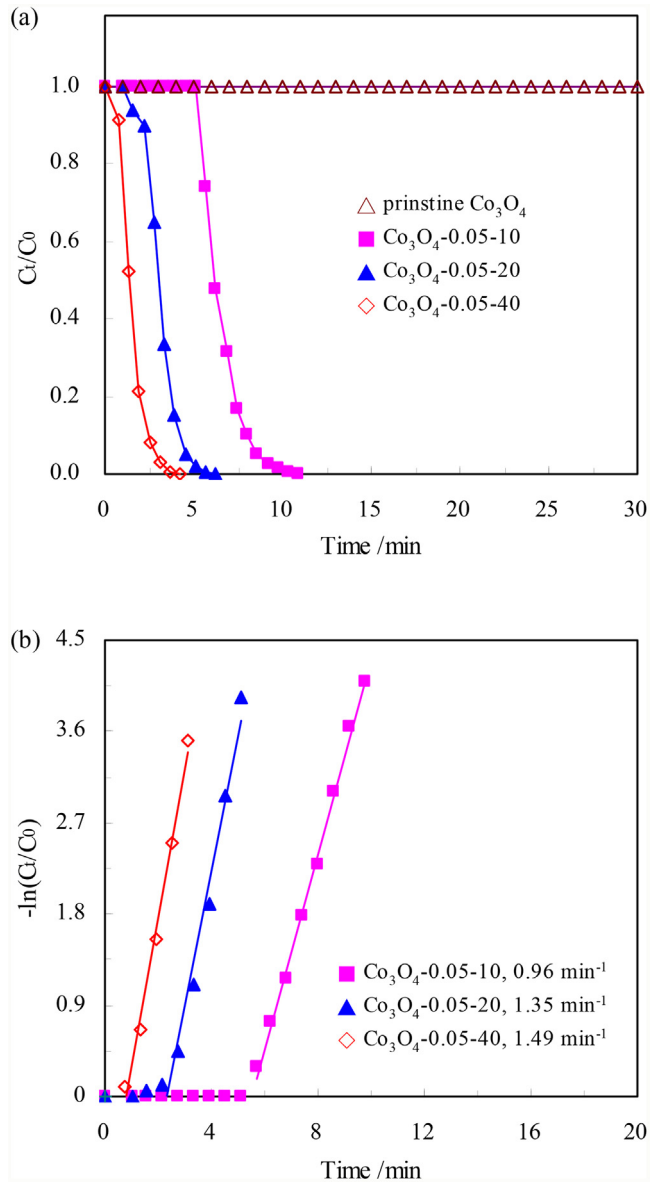


Fig. 6. (a) C_t/C_0 as a function of reaction time (b) kinetic analysis over Co_3O_4 reduced for different times. $C_{\text{p-NP}} = 0.125 \text{ mmol/L}$, $\text{p-NP}/\text{NaBH}_4 = 100$, $m_{\text{cat}} = 0.2 \text{ mg}$.

and catalyst amount on the catalytic activity of reduced Co_3O_4 were studied in detail.

3.2.1. Effect of the reduction time

Firstly, the catalytic reduction of p-NP to p-AP by NaBH_4 was carried out over Co_3O_4 reduced for different times. The molar ratio of NaBH_4 to p-NP was fixed at 100 to obtain a pseudo-first-order kinetic behavior. The zeta potentials of pristine Co_3O_4 and Co_3O_4 reduced for different times were measured and the values were between -14.8 and -12.5 mV (Table S1). Obviously, the suspensions of pristine Co_3O_4 or Co_3O_4 reduced for different times corresponded to the unstable dispersion [51]. To investigate the stability of the suspension of reduced Co_3O_4 schematically, the photograph of the suspension of Co_3O_4 -0.05-40 was taken at different times. The suspension showed no obvious change within 30 min, indicating that the dispersion of reduced Co_3O_4 had little change during the catalytic reduction of p-NP (Fig. S3). Fig. 6a displays C_t/C_0 as a function of reaction time, where C_t and C_0 represent the concentration of p-NP at a certain time point and initial

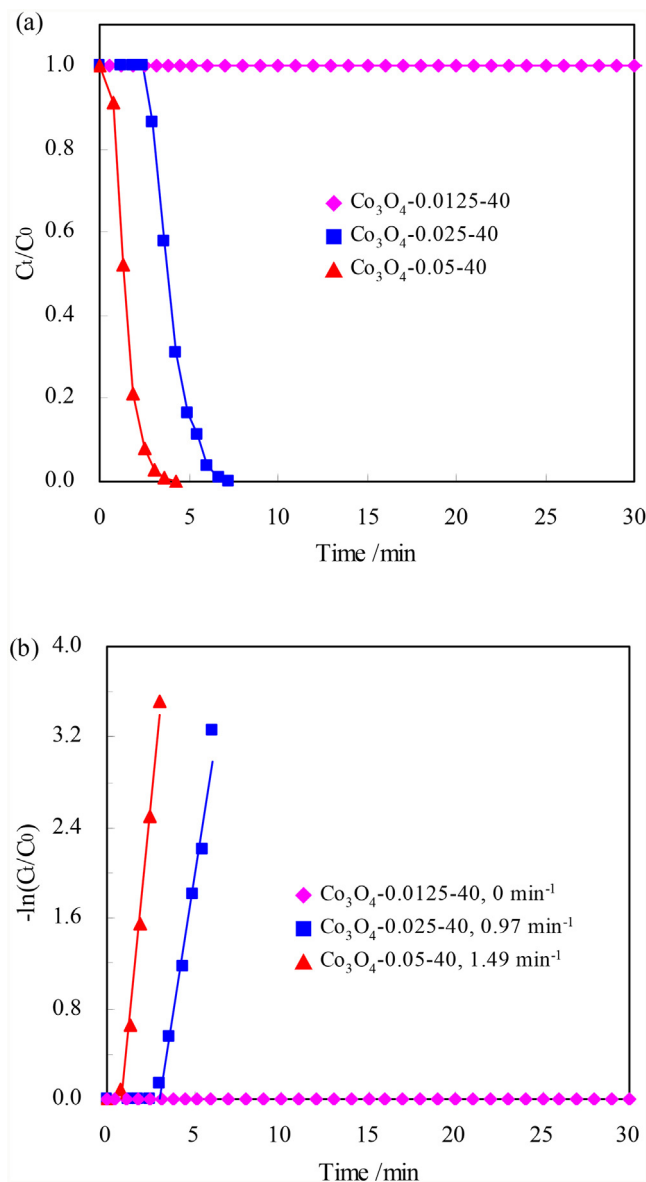


Fig. 7. (a) C_t/C_0 as a function of reaction time (b) kinetic analysis over Co_3O_4 reduced by aqueous NaBH_4 with different concentrations. $\text{C}_{\text{p-NP}} = 0.125 \text{ mmol/L}$, $\text{p-NP}/\text{NaBH}_4 = 100$, $m_{\text{cat}} = 0.2 \text{ mg}$.

Table 3
The induction time of Co_3O_4 reduced for different times.

Catalyst	$\text{Co}_3\text{O}_4\text{-}0.05\text{-}10$	$\text{Co}_3\text{O}_4\text{-}0.05\text{-}20$	$\text{Co}_3\text{O}_4\text{-}0.05\text{-}40$
t_0/min	$5.08 < t_0 < 5.67$	$1.00 < t_0 < 1.58$	$t_0 < 0.75$

concentration of p-NP, respectively. It can be seen that pristine Co_3O_4 shows no catalytic activity towards the reduction of p-NP within 30 min. Excitingly, the catalytic performance is dramatically improved over $\text{Co}_3\text{O}_4\text{-}0.05\text{-}Y$ ($Y = 10, 20$ and 40 min). It is obvious that there is an induction time (t_0) in which no reduction occurs over $\text{Co}_3\text{O}_4\text{-}0.05\text{-}Y$ ($Y = 10, 20$ and 40 min). Afterward, the reduction process proceeds quickly. The induction time of $\text{Co}_3\text{O}_4\text{-}0.05\text{-}Y$ ($Y = 10, 20$ and 40 min) is summarized in Table 3. It can be found that the induction time decreases significantly with the increasing reduction time. The existence of induction time has been widely found. Some studies attributed the induction time to the diffusion barrier [14], whereas the others suggested that the induction time was related to the spontaneous surface reconstruction [13,52]. Up

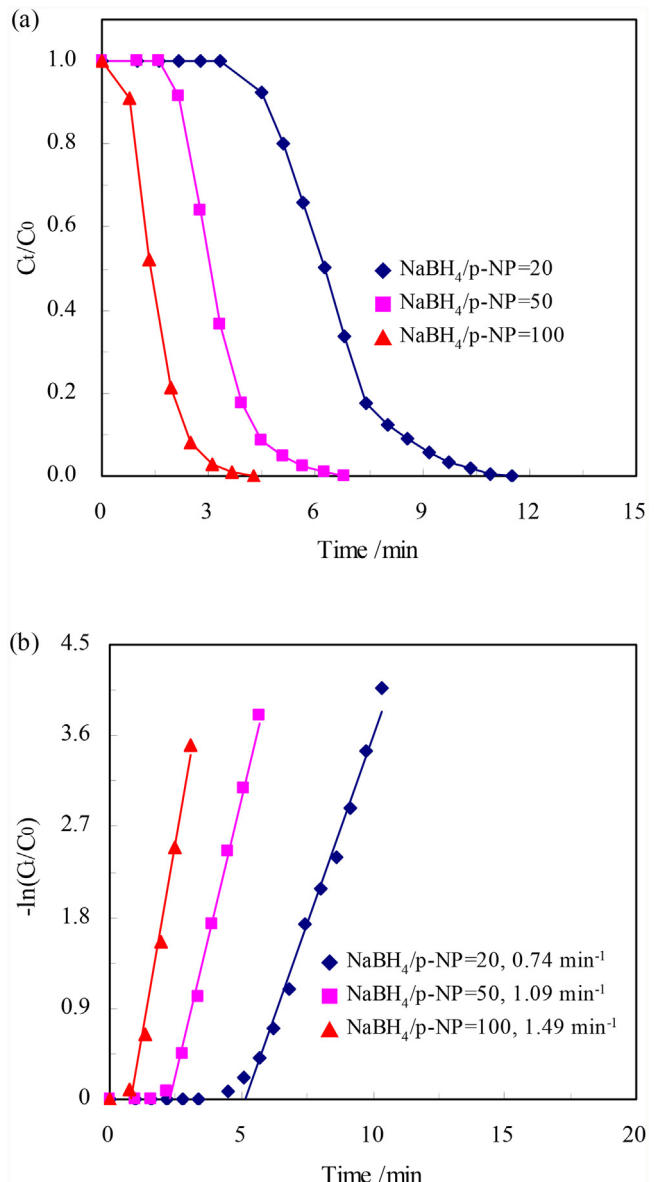


Fig. 8. (a) C_t/C_0 as a function of reaction time (b) kinetic analysis over $\text{Co}_3\text{O}_4\text{-}0.05\text{-}40$ at different molar ratios of NaBH_4 to p-NP. $\text{C}_{\text{p-NP}} = 0.125 \text{ mmol/L}$, $m_{\text{cat}} = 0.2 \text{ mg}$.

to now, the reason for the induction time is still unclear and an issue of debate. The common consensus is that the catalyst with the best catalytic activity possesses the shortest induction time. In this study, because the BET surface areas and pore properties of $\text{Co}_3\text{O}_4\text{-}0.05\text{-}Y$ ($Y = 10, 20$ and 40 min) are similar, it can be predicted that the diffusion barriers are comparable for these catalysts. Therefore, the diffusion barrier is not the major factor which results in the induction time. The reason for the induction phenomenon over $\text{Co}_3\text{O}_4\text{-}0.05\text{-}Y$ ($Y = 10, 20$ and 40 min) will be discussed in later section.

In order to evaluate the catalytic activity of $\text{Co}_3\text{O}_4\text{-}0.05\text{-}Y$ ($Y = 10, 20$ and 40 min), the kinetic analysis was carried out. As a typical model reaction, the kinetics of the catalytic reduction of p-NP to p-AP by NaBH_4 has been extensively investigated [52–54]. Langmuir–Hinshelwood model is always employed to conduct the kinetic analysis. In this model, the reduction reaction proceeds in three stages: (1) p-NP molecules are adsorbed on the catalyst surface. At the same time, borohydride ions are competitively adsorbed on the catalyst surface, react with the surface, and transfer

surface-hydrogen species to the surface. All steps involving in this stage are reversible and assumed to be fast; (2) The adsorbed p-NP molecules and surface-hydrogen species react to form p-AP; (3) The generated p-AP is desorbed from the catalyst surface. Among these stages, the reduction of adsorbed p-NP by the surface-hydrogen species is considered as the rate-determining step.

When a large excess of NaBH₄ is used, the reduction of p-NP to p-AP can be seen as a pseudo-first-order reaction:

$$-\ln(C_t/C_0) = k_{app}(t - t_0) \quad (1)$$

where k_{app} and t represent the apparent rate constant and reaction time, respectively. Therefore, the slope of the linear curve ($(t - t_0)$ versus $-\ln(C_t/C_0)$) represents the apparent rate constant. As shown in Fig. 6b, the kinetic behaviors over reduced Co₃O₄ strictly follow the pseudo-first-order reaction. In contrary to the induction time, the rate constant of reduced Co₃O₄ increases with the increase in reduction time. The apparent rate constants of Co₃O₄-0.05-Y (Y = 10, 20 and 40 min) are 0.96, 1.35 and 1.49 min⁻¹, respectively. Apparently, Co₃O₄-0.05-40 exhibits the best performance in term of the shortest induction time and highest apparent rate constant. For the metal oxide catalysts including Co₃O₄, the catalytic performance is usually closely associated with the morphology, crystallinity, specific surface area and surface properties, etc [55–57]. From the characterization results of XRD, N₂ physisorption, TEM and SEM, pristine Co₃O₄ and Co₃O₄-0.05-Y (Y = 10, 20 and 40 min) exhibited similar crystallinity, specific surface area, pore properties and morphology. Hence, the difference in the catalytic activities of Co₃O₄-0.05-Y (Y = 10, 20 and 40 min) cannot be contributed to the aforementioned factors. The catalytic activity of reduced Co₃O₄ might be closely related with the surface properties. The XPS analysis demonstrated annealing pristine Co₃O₄ in aqueous NaBH₄ resulted in the formation of oxygen vacancies. Generally, the oxygen vacancies can be empty (V_O²⁺), occupied by one electron (V_O⁺) or two electrons (V_O⁰). According to DFT calculation, the oxygen vacancies were likely formed as V_O²⁺ due to the lowest formation energy [48]. Compared to pristine Co₃O₄, the positive surface charge (V_O²⁺) enabled reduced Co₃O₄ to adsorb more p-NP anions and BH₄⁻ anions, and thus resulted in a higher catalytic activity. Konar et al. also demonstrated the enhancement effect of positive surface charge of CuO nanostars on the reduction of p-NP by NaBH₄ [7]. In addition, the amount of oxygen vacancies increased with the increasing reduction time. This trend was similar with the catalytic activities of Co₃O₄-0.05-Y (Y = 10, 20 and 40 min), which further confirmed that the catalytic activity was dependent on the amount of oxygen vacancies.

3.2.2. The effect of NaBH₄ concentration used for catalyst preparation

Fig. 7 shows the effect of NaBH₄ concentration used for catalyst preparation on the catalytic activity of reduced Co₃O₄. It can be seen that Co₃O₄ reduced in 0.0125 mol/L NaBH₄ shows no activity within 30 min. When the NaBH₄ concentration is increased to 0.025 mol/L, the reduction of p-NP to p-AP proceeds quickly after an induction time smaller than 3 min. 100% p-NP is transformed into p-AP within 7.25 min and the rate constant is calculated to be 0.97 min⁻¹. As the NaBH₄ concentration is increased to 0.05 mol/L, the catalytic activity is further enhanced. The induction time and rate constant are <0.75 min and 1.49 min⁻¹, respectively. Evidently, the NaBH₄ concentration used for catalyst preparation plays a vital role for preparing highly active catalysts. The difference in the catalytic activities of Co₃O₄-X-40 (X = 0.0125, 0.025 and 0.05 mol/L) can be attributed to the dissimilar amount of oxygen vacancies on the surface of reduced Co₃O₄. It can be predicted that the amount of oxygen vacancies goes up with the increasing NaBH₄ concentration

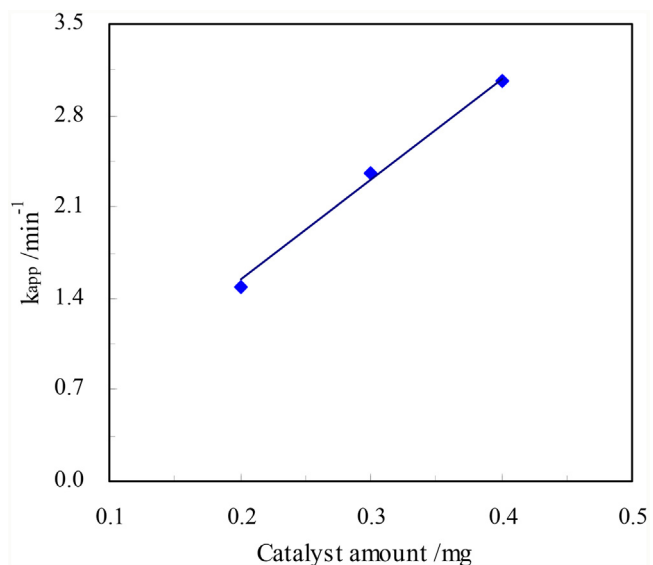


Fig. 9. The effect of catalyst amount on the apparent rate constant of Co₃O₄-0.05-40. C_{p-NP} = 0.125 mmol/L, p-NP/NaBH₄ = 100.

due to the stronger reducibility of aqueous NaBH₄ used for catalyst preparation.

3.2.3. The effect of the molar ratio of NaBH₄ to p-NP

The effect of the molar ratio of NaBH₄ to p-NP on the catalytic activity of reduced Co₃O₄ was investigated. In this section, the molar ratio of NaBH₄ to p-NP varied from 20 to 100, while the concentration of p-NP was kept unchanged. Fig. 8a shows C_t/C_0 as a function of the reaction time over Co₃O₄-0.05-40. It can be seen that the induction time decreases significantly with the increasing molar ratio of NaBH₄ to p-NP. As discussed above, the induction time over reduced Co₃O₄ was independent on the diffusion barrier. Herein, the induction phenomenon of the catalyst seemed to correlate with NaBH₄. In order to verify this hypothesis, 0.7 mL of NaBH₄ aqueous solution and 0.2 mg of Co₃O₄-0.05-40 was mixed firstly. After 1 min, 2 mL of p-NP aqueous solution was added into this suspension. As presented in Fig. S4, the induction time is remarkably decreased as compared to conventional protocol (NaBH₄ and p-NP solutions mixed together before the addition of Co₃O₄-0.05-40) at the molar ratio of NaBH₄ to p-NP of 20 and 50. As stated in Section 3.2.1, oxygen vacancies generated during the surface reduction process were considered as the active sites of reduced Co₃O₄. A few literature studies demonstrated the surface oxygen defects were not usually stable enough to survive in air and were even susceptible to oxidation by dissolved oxygen in water [58–60]. In our experimental, the reduced Co₃O₄ was washed several times with deionized water before being used for the catalytic reduction of p-NP. During the washing process, the dissolved oxygen in deionized water might adsorb on the oxygen vacancies of reduced Co₃O₄. Hence, the induction time might be caused by the desorption of adsorbed oxygen from the oxygen vacancies by NaBH₄. This was in consistent with the experimental results that the induction time decreased with the increasing molar ratio of NaBH₄ to p-NP.

The kinetic curves of Co₃O₄-0.05-40 at different molar ratios of NaBH₄ to p-NP are depicted in Fig. 8b. It can be seen that the apparent rate constant increases with the increasing molar ratio of NaBH₄ to p-NP. As mentioned above, borohydride ions and p-NP molecules compete for the same active sites on the catalyst surface. The reaction can only happen between the adsorbed species. Accordingly, if most active sites are occupied by one species, the reaction will be hindered dramatically. On the basis of the kinetic studies of noble metal NPs such as Au, Pt and AuPd alloy, the adsorption equilib-

Table 4The mass-normalized rate constants of different catalysts for the catalytic reduction of p-NP to p-AP by NaBH₄.

Catalyst	C _{p-NP}	C _{NaBH₄}	m _{cat}	k _{app}	k _{nor} ^a	Reference
	mmol/L	mmol/L	g/L	min ⁻¹	min ⁻¹ g ⁻¹ L	
Au ligands	0.10	49.95	0.000049	0.196	4000.00	[23]
Au ₅₃ Pd ₄₇ NPs/GNS	0.05	5	0.0006	0.87	1387.20	[29]
Pt3Au1-PDA/RGO	0.09	10	0.020	0.57	28.74	[25]
AuPt@Au	0.23	333.33	0.033	0.52	15.66	[61]
Au/graphene oxide	0.05	100.00	0.170	0.59	3.47	[21]
Cu ₂ O@CuO/Au-Pd	0.06	4.95	0.099	1.16	11.72	[26]
Au-CeO ₂ @ZrO ₂	0.08	0.93	0.034	1.45	42.35	[27]
rGO/Fe ₃ O ₄ /Au	0.08	65.57	1.311	0.69	0.52	[62]
Au@ mesoporous SnO ₂	0.08	0.71	0.033	0.09	2.82	[28]
SnO ₂	0.11	10.57	1.511	0.05	0.04	[63]
CoMnO ₄	0.07	6.67	0.047	0.90	19.22	[64]
NiCo alloy	0.03	20.00	0.033	0.07	2.20	[34]
Co-NCC	0.17	13.44	0.270	2.82	10.44	[65]
Co@SiO ₂	0.60	60.00	0.200	0.82	4.08	[33]
meso-Co ₃ O ₄	0.04	10.00	0.080	~0.018	0.23	[36]
reduced Co ₃ O ₄	0.125	12.50	0.071	1.49	20.86	this work

^a The mass-normalized rate constant was calculated based on the catalyst amount including the support.

rium constant of p-NP is always 10 times larger than that of NaBH₄ [52–54]. For example, the adsorption equilibrium constants of p-NP and NaBH₄ were 3000 and 170 L mol⁻¹ over SPB-Au₇₅Pd₂₅, respectively [54]. Apparently, the adsorption of p-NP molecules is much stronger than that of NaBH₄. Therefore, as the molar ratio of NaBH₄ to p-NP increases in a certain range, the number of adsorbed borohydride ions as well as the reaction probability between adsorbed p-NP molecules and surface-hydrogen species transformed from adsorbed borohydride ions go up. Correspondingly, the apparent rate constant increases with the increasing molar ratio of NaBH₄ to p-NP.

3.2.4. The effect of catalyst amount

It can be learnt from Langmuir-Hinshelwood model that the apparent rate constant is linearly related to the total surface area of the catalyst. Accordingly, the apparent rate constant will be linearly dependent on the catalyst amount when the same catalyst is used. Fig. 9 shows the effect of catalyst amount on the apparent rate constant of Co₃O₄-0.05-40. It can be seen that the apparent rate constant linearly increases with the increase in catalyst amount. As the catalyst amount increases from 0.2 mg to 0.4 mg, the apparent rate constant increases from 1.49 min⁻¹ to 3.01 min⁻¹.

3.2.5. Stability test

The development of the catalyst with good reusability is one of the most important goals for practical application. In this section, the reusability of reduced Co₃O₄ was evaluated by successive addition of concentrated p-NP aqueous solution after each cycle. The concentration of p-NP in the quartz cell before reaction was adjusted to 0.125 mmol/L. The molar ratio of NaBH₄ to p-NP was 100 in the first cycle, and no NaBH₄ was supplemented in the following cycles. As shown in Fig. 10, the apparent rate constant of Co₃O₄-0.05-40 shows no obvious deactivation after five successive cycles, indicating that Co₃O₄-0.05-40 possesses good stability for the catalytic reduction of p-NP to p-AP by NaBH₄. Since the apparent rate constant is related to the catalyst amount, the mass-normalized rate constant (k_{nor}) is usually employed to compare the activities of different catalysts. The definition of mass-normalized rate constant is stated as Eq. (2):

$$k_{nor} = k_{app}/m_{cat} \quad (2)$$

The mass-normalized rate constants of different catalysts are summarized in Table 4. It should be pointed out that when comparing the catalytic activity, the concentrations of p-NP and NaBH₄ also need to be considered because of their effects on the apparent

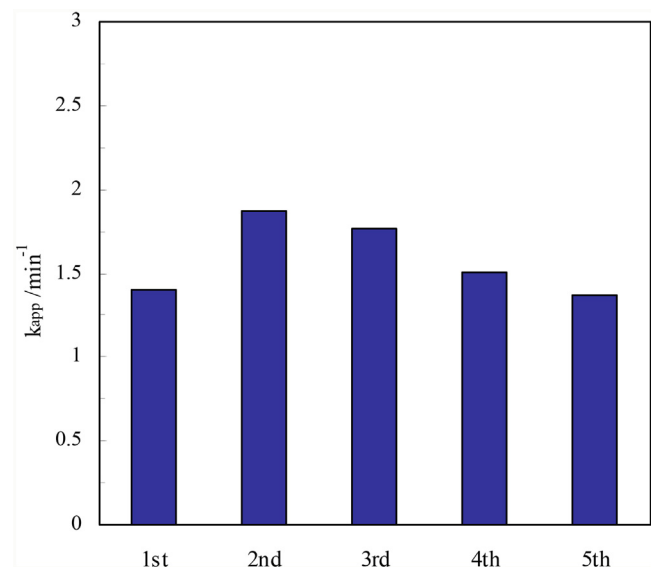


Fig. 10. The reusability of Co₃O₄-0.05-40 for the catalytic reduction of p-NP to p-AP by NaBH₄. C_{p-NP} = 0.125 mmol/L, m_{cat} = 0.2 mg.

rate constant. It can be seen from Table 4 that the catalytic activity of Co₃O₄-0.05-40 is comparable with those of supported noble metal catalysts such as Au/graphene oxide, Au@SnO₂ and rGO/Fe₃O₄/Au, etc.

4. Conclusion

In summary, reduced Co₃O₄ was easily prepared by a facile surface reduction with aqueous NaBH₄ at 30 °C. In the catalytic reduction of p-NP to p-AP by NaBH₄, pristine Co₃O₄ showed no catalytic activity within 30 min, while the performance of reduced Co₃O₄ was excellent. The characterization results revealed that the superior activity of reduced Co₃O₄ was attributed to the oxygen vacancies formed during the surface reduction process. The reduction time and NaBH₄ concentration used for catalyst preparation was found to affect the catalytic activity of reduced Co₃O₄ significantly. Co₃O₄ reduced in 0.05 mol/L aqueous NaBH₄ for 40 min exhibited the best catalytic activity. Additionally, the as-prepared reduced Co₃O₄ showed no obvious deactivation in five successive cycles. Considering the easy preparation, low cost, good activity

and reusability, reduced Co_3O_4 can serve as a potential catalyst for the catalytic reduction of p-NP to p-AP by NaBH_4 .

Acknowledgement

The authors gratefully acknowledge the financial support from National Natural Science Foundation of China (Nos. 21406226, 21225627).

Appendix A. Supplementary data

Supplementary data associated with this article can be found, in the online version, at <http://dx.doi.org/10.1016/j.apcatb.2017.03.038>.

References

- [1] S. Yi, W.Q. Zhuang, B. Wu, S.T.L. Tay, J.H. Tay, *Environ. Sci. Technol.* 40 (2006) 2396–2401.
- [2] S.Q. Yu, J. Hu, J.L. Wang, *J. Hazard. Mater.* 177 (2010) 1061–1067.
- [3] S. Gao, Z.Y. Zhang, K.C. Liu, B. Dong, *Appl. Catal. B: Environ.* 188 (2016) 245–252.
- [4] Z.P. Dong, X.D. Le, C.X. Dong, W. Zhang, X.L. Li, J.T. Ma, *Appl. Catal. B: Environ.* 162 (2015) 372–380.
- [5] K. Karakas, A. Celebioglu, M. Celebi, T. Uyar, M. Zahmakiran, *Appl. Catal. B: Environ.* 203 (2017) 549–562.
- [6] Y.S. Fu, T. Huang, L.L. Zhang, J.W. Zhu, X. Wang, *Nanoscale* 7 (2015) 13723–13733.
- [7] S. Konar, H. Kalita, N. Puvvada, S. Tantubay, M.K. Mahto, S. Biswas, A. Pathak, *J. Catal.* 336 (2016) 11–22.
- [8] Y.S. Fu, T. Huang, B.Q. Jia, J.W. Zhu, X. Wang, *Appl. Catal. B: Environ.* 202 (2017) 430–437.
- [9] G.Z. Li, Y.J. Jiang, D.L. Chen, J. Li, S.X. Lu, *J. Catal.* 317 (2014) 83–90.
- [10] M.Z. Guo, J. He, Y. Li, S. Ma, X.H. Sun, *J. Hazard. Mater.* 310 (2016) 89–97.
- [11] B.K. Barman, K.K. Nanda, *Dalton Trans.* 44 (2015) 4215–4222.
- [12] A.M. Kalekar, K.K.K. Sharma, M.N. Luwang, G.K. Sharma, *RSC Adv.* 6 (2016) 11911–11920.
- [13] A.M. Kalekar, K.K.K. Sharma, A. Lehoux, F. Audonnet, H. Remita, A. Saha, G.K. Sharma, *Langmuir* 29 (2013) 11431–11439.
- [14] J. Zeng, Q. Zhang, J.Y. Chen, Y.N. Xia, *Nano Lett.* 10 (2010) 30–35.
- [15] Y. Zhang, Z.M. Cui, L.D. Li, L. Guo, S.H. Yang, *Phys. Chem. Chem. Phys.* 17 (2015) 14656–14661.
- [16] J.Z. Min, F. Wang, Y.L. Cai, S. Liang, Z.W. Zhang, X.M. Jiang, *Chem. Commun.* 51 (2015) 761–764.
- [17] Z.F. Jiang, D.L. Jiang, A.M.S. Hossain, K. Qian, J.M. Xie, *Phys. Chem. Chem. Phys.* 17 (2015) 2550–2559.
- [18] C. Lin, K. Tao, D.Y. Hua, Z. Ma, S.H. Zhou, *Catal. Lett.* 144 (2014) 1001–1008.
- [19] T. Zeng, X.L. Zhang, S.H. Wang, Y.R. Ma, H.Y. Niu, Y.Q. Cai, *J. Mater. Chem. A* 1 (2013) 11641–11647.
- [20] X. Huang, X.P. Liao, B. Shi, *Green Chem.* 13 (2011) 2801–2805.
- [21] M.M. Zhang, X. Lu, H.Y. Wang, X.L. Liu, Y.J. Qin, P. Zhang, Z.X. Guo, *RSC Adv.* 6 (2016) 35945–35951.
- [22] M.B. Li, S.K. Tian, Z.K. Wu, R.C. Jin, *Chem. Commun.* 51 (2015) 4433–4436.
- [23] Y. Dai, P. Yu, X.J. Zhang, R.X. Zhuo, *J. Catal.* 337 (2016) 65–71.
- [24] S.M. Ansar, C.L. Kitchens, *ACS Catal.* 6 (2016) 5553–5560.
- [25] W.C. Ye, J. Yu, Y.X. Zhou, D.Q. Gao, D.A. Wang, C.M. Wang, D.S. Xue, *Appl. Catal. B: Environ.* 181 (2016) 371–378.
- [26] W. Yao, F.L. Li, H.X. Li, J.P. Lang, *J. Mater. Chem. A* 3 (2015) 4578–4585.
- [27] V. Evangelista, B. Acosta, S. Miridonov, E. Smolentseva, S. Fuentes, A. Simakov, *Appl. Catal. B: Environ.* 166 (2015) 518–528.
- [28] Y. Wang, L. Li, C.G. Wang, T.T. Wang, *J. Nanopart. Res.* 18 (2015) 2.
- [29] X.M. Chen, Z.X. Cai, X. Chen, M. Oyama, *J. Mater. Chem. A* 2 (2014) 5668–5674.
- [30] Y. Ma, X.Y. Wu, G.K. Zhang, *Appl. Catal. B: Environ.* 205 (2017) 262–270.
- [31] N. Sahiner, H. Ozay, O. Ozay, N. Aktas, *Appl. Catal. B: Environ.* 101 (2010) 137–143.
- [32] H.Y. Ma, H.T. Wang, T. Wu, C.Z. Na, *Appl. Catal. B: Environ.* 180 (2016) 471–479.
- [33] N. Yan, Z. Zhao, Y. Li, F. Wang, H. Zhong, Q.W. Chen, *Inorg. Chem.* 53 (2014) 9073–9079.
- [34] K.L. Wu, X.W. Wei, X.M. Zhou, D.H. Wu, X.W. Liu, Y. Ye, Q. Wang, *J. Phys. Chem. C* 115 (2011) 16268–16274.
- [35] T.R. Mandlimath, B. Gopal, *J. Mol. Catal. A: Chem.* 350 (2011) 9–15.
- [36] B.M. Mogudi, P. Ncube, R. Meijboom, *Appl. Catal. B: Environ.* 198 (2016) 74–82.
- [37] J. Su, X.X. Zou, J.S. Chen, *RSC Adv.* 4 (2014) 13979–13988.
- [38] G.M. Wang, H.Y. Wang, Y.C. Ling, Y.C. Tang, X.Y. Yang, R.C. Fitzmorris, C.C. Wang, J.Z. Zhang, Y. Li, *Nano Lett.* 11 (2011) 3026–3033.
- [39] B. Bharti, S. Kumar, H.N. Lee, R. Kumar, *Sci. Rep.* 6 (2016) 32355.
- [40] Y.X. Pan, Z.Q. Sun, H.P. Cong, Y.L. Men, S. Xin, J. Song, S.H. Yu, *Nano Res.* 9 (2016) 1689–1700.
- [41] G.M. Wang, Y.C. Ling, H.Y. Wang, X.Y. Yang, C.C. Wang, J.Z. Zhang, Y. Li, *Energy Environ. Sci.* 5 (2012) 6180–6187.
- [42] Q. Kang, J.Y. Cao, Y.J. Zhang, L.Q. Liu, H. Xu, J.H. Ye, *J. Mater. Chem. A* 1 (2013) 5766–5774.
- [43] D.D. Qin, T. Wang, Y.M. Song, C.L. Tao, *Dalton Trans.* 43 (2014) 7691–7694.
- [44] M. Kang, M.W. Song, C.H. Lee, *Appl. Catal. A: Gen.* 251 (2003) 143–156.
- [45] J.Y. Luo, M. Meng, X. Li, X.G. Li, Y.Q. Zha, T.D. Hu, Y.N. Xie, J. Zhang, *J. Catal.* 254 (2008) 310–324.
- [46] L.F. Liotta, G. Di Carlo, G. Pantaleo, A.M. Venezia, G. Deganello, *Appl. Catal. B: Environ.* 66 (2006) 217–227.
- [47] W.Q. Song, A.S. Poyraz, Y.T. Meng, Z. Ren, S.Y. Chen, S.L. Suib, *Chem. Mater.* 26 (2014) 4629–4639.
- [48] Y.C. Wang, T. Zhou, K. Jiang, P.M. Da, Z. Peng, J. Tang, B.A. Kong, W.B. Cai, Z.Q. Yang, G.F. Zheng, *Adv. Energy Mater.* 4 (2014), 1400696.
- [49] T.L. Pfeil, T.L. Pourpoint, L.J. Groven, *Int. J. Hydrogen Energy* 39 (2014) 2149–2159.
- [50] O.V. Komova, V.I. Simagina, O.V. Netskina, D.G. Kellerman, A.V. Ishchenko, N.A. Rudina, *Catal. Today* 138 (2008) 260–265.
- [51] S. Vallar, D. Houivet, J. El Fallah, D. Kervadec, J.M. Haussonne, *J. Eur. Ceram. Soc.* 19 (1999) 1017–1021.
- [52] S. Wunder, Y. Lu, M. Albrecht, M. Ballauff, *ACS Catal.* 1 (2011) 908–916.
- [53] S. Wunder, F. Polzer, Y. Lu, Y. Mei, M. Ballauff, *J. Phys. Chem. C* 114 (2010) 8814–8820.
- [54] S. Gu, Y. Lu, J. Kaiser, M. Albrecht, M. Ballauff, *Phys. Chem. Chem. Phys.* 17 (2015) 28137–28143.
- [55] M. Yang, Y. Men, S.L. Li, G.W. Chen, *Appl. Catal. A: Gen.* 433 (2012) 26–34.
- [56] X.L. Ouyang, S.L. Li, J. Yue, F.J. Jiao, G.W. Chen, *Int. J. Global Warm.* 1 (2009) 456–472.
- [57] H.H. Chen, M. Yang, S. Tao, M.Y. Ren, G.W. Chen, *Cryst. Growth Des.* 16 (2016) 6286–6293.
- [58] F. Zuo, K. Bozhilov, R.J. Dillon, L. Wang, P. Smith, X. Zhao, C. Bardeen, P.Y. Feng, *Angew. Chem. Int. Ed.* 124 (2012) 6327–6330.
- [59] K. Komaguchi, T. Maruoka, H. Nakano, I. Imae, Y. Ooyama, Y. Harima, *J. Phys. Chem. C* 114 (2010) 1240–1245.
- [60] A. Teleki, S.E. Pratsinis, *Phys. Chem. Chem. Phys.* 11 (2009) 3742–3747.
- [61] Q. Liu, Y.R. Xu, A.J. Wang, J.J. Feng, *RSC Adv.* 5 (2015) 96028–96033.
- [62] Y. Wang, H. Li, J.J. Zhang, X.Y. Yan, Z.X. Chen, *Phys. Chem. Chem. Phys.* 18 (2016) 615–623.
- [63] A. Bhattacharjee, M. Ahmaruzzaman, *Mater. Lett.* 157 (2015) 260–264.
- [64] X.H. Shi, F.C. Zheng, N. Yana, Q.W. Chen, *Dalton Trans.* 43 (2014) 13865–13873.
- [65] Z. Hasan, D.W. Cho, C.M. Chon, K. Yoon, H. Song, *Chem. Eng. J.* 298 (2016) 183–190.